# Self-Assembly of Emissive Nanocellulose/Quantum Dots Nanostructures for Chiral Fluorescent Materials

Rui Xiong,† Shengtao Yu,† Marcus J. Smith,† Jing Zhou,† Michelle Krecker,† Lijuan Zhang,† Dhriti Nepal,‡ Timothy J. Bunning,‡ Vladimir V. Tsukruk†\*

† School of Materials Science and Engineering, Georgia Institute of Technology, Atlanta, Georgia 30332-0245, United States

‡ Air Force Research Laboratory, Materials and Manufacturing Directorate, Wright Patterson Air Force Base, OH, 45433, United States

#### **Abstract**

Chiral fluorescent materials with fluorescent nanoparticles assembled into chiral structure represent a grand challenge. Here, we report self-assembled emissive needle-like nanostructures through decorating cellulose nanocrystals (CNCs) with carbon quantum dots (CQDs). This assembly is facilitated by the heterogeneous amphiphilic interactions between natural and synthetic components. These emissive nanostructures can self-organize into chiral nematic solid-state materials with enhanced mechanical performance. The chiral CQDs/CNC films demonstrate an intense iridescent appearance superimposed with enhanced luminescence that is significantly higher than that for CQDs film and other reported CQDs/CNC films. Notably, characteristic fluorescent fingerprint signature is observed in the CQDs/CNC film, proving the well-defined chiral organization of fluorescent nanostructures. The chiral organization of CQDs enables the solid CQDs/CNC film right-hand chiral fluorescence with an asymmetric factor of -0.2. Additionally, we developed a chemical 2D printing and soft-lithography patterning techniques to fabricate the fluorescent patterns, which can combine the high mechanical integrity and freestanding ability, as well as chiral nematic structure with light diffraction and emission.

**Key words**: cellulose nanocrystals; carbon quantum dots; chiral fluorescence; self-assembly; fluorescent patterns; liquid crystals; photonic structures; mechanical properties

\*E-mail: vladimir@mse.gatech.edu

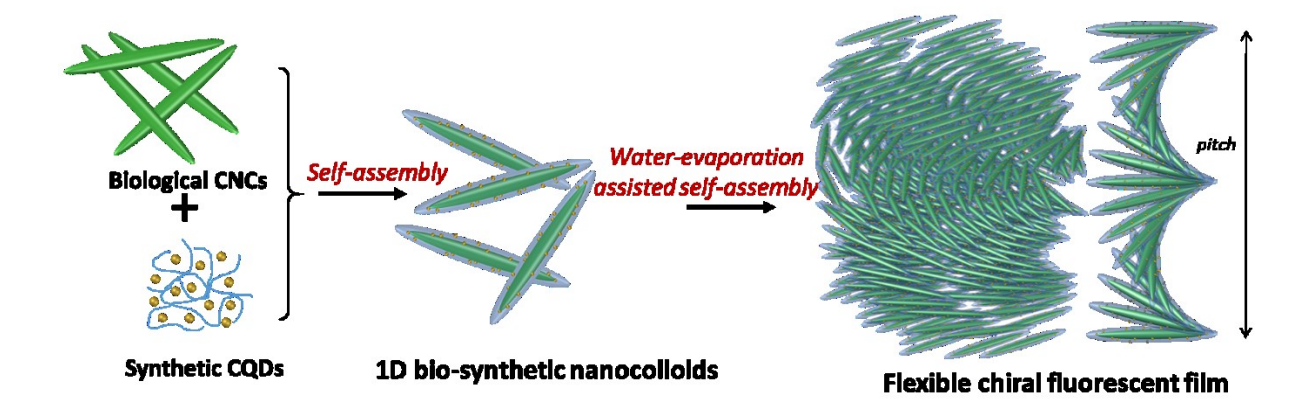
Assembling optically active chiral bionanocomposites that are light-weight, flexible, and mechanically robust attracts wide interest due to their great potential in chiral catalysis, biolasing, chiral sensing, and polarization-enabled optoelectronic applications. Significant progress has been achieved in the assembly of metal nanoparticles (NPs), semiconductor NPs, and nanocarbon structures into nanoscale chiral geometries (*e.g.*, twisted pairs, pyramids, and helices) by templating with chiral biological components, such as amino acids and DNAs. However, very few successful examples have been demonstrated for extending these concepts to macroscopic robust chiral bioenabled optical systems from biotic-abiotic materials that are promising for advanced optical applications. Current systems are limited because of their complex non-uniform organization and suppressed chiral optical activity upon mixing with additional components.

Needle-like cellulose nanocrystals (CNCs) are naturally occurring one-dimensional (1D) nanostructures with a high aspect ratio and natural chirality. 9,10 CNCs possess high crystalline order, prominent chirality, superior elastic modulus (150 GPa), and diverse surface chemistry. 11-14 The well-defined chirality and excellent dispersion stability of CNCs allow them to spontaneously assemble into a left-handed chiral nematic liquid crystal (LC) phase in concentrated dispersions that can be preserved into a solid film upon solvent evaporation under carefully-controlled processing conditions. 15,16 The resulting helicoidal organization endows CNC films with brilliant iridescent structural colors due to selective visible light reflection with prominent circular polarization. 17,18 Such chiral behavior can be utilized to guide the assembly of synthetic optical components for constructing chiral biophotonic materials. 19-23 Additionally, patterning these chiral films can lead to additional optical functionalities such as photonic cholesteric films with omnidirectional lasing and broadband reflection. 24

Examples of optically active bionanocomposites have been demonstrated by combining chiral CNC matrix with plasmonic and luminescent NPs, including gold NPs, quantum dots, latex NPs, and rare-earth NPs. 20-23,25-27 Low NP loading (below 0.5 wt% in order to avoid phase separation) and huge size difference in components, however, typically leads to NPs randomly and sparsely doped CNC matrix without chiral organization. As a result, these composites demonstrate suppressed structural colors, low luminescence, and poor mechanical strength. 20,23-26,28 To date, the assembly of CNCs with fluorescent NPs for realizing chiral organization of emissive NPs remains a grand challenge commonly due to severe phase separation. For instance, co-assembly of fluorescent latex-NPs and CdS quantum dots (QDs) into chiral CNC matrix results in strong fluorescence, 20,25 but these NPs are randomly distributed. Chirality as observed from circular dichroism (CD) measurements usually originates solely from the host CNC matrix or

randomly dispersed CNC tactoids. In other attempts, carbon quantum dots (CQDs) are adopted to assemble with CNCs because of their minute size (around 1 nm), diverse functionalities, water solubility, and low toxicity.<sup>27,29</sup> However, the resulting CQDs/CNC films are extremely brittle, with low or even completely absent emission due to quenching of aggregated CQDs.<sup>25</sup>

Here, we report highly emissive CQDs/CNC nanostructures ("nanocobs") composed of polymer stabilized luminescent CQDs nanoshells assembled around individual CNC (Scheme 1). These 1D fluorescent core/shell nanostructures are capable of assembling into chiral LC organization without any signs of phase separation with bright structural colors. This organization stabilizes the CQDs and prevents their aggregation and quenching for high emission that that is two-order higher than pure CQDs film and much higher than that reported for other CQDs/CNC films<sup>27,29</sup> The chiral organization also provide the solid CQDs/CNC film with right-hand chiral fluorescence with an asymmetric factor of -0.2. Additionally, the balanced interfacial interaction between CQDs and CNC enhanced the toughness and flexibility of the chiral fluorescent films. To the best of our knowledge, the combination of highly emissive chiral luminescence with robust mechanical properties has never achieved in previous chiral fluorescent CNC composites that usually suffer from suppressed fluorescence and excessive brittleness. Furthermore, a characteristic chiral fluorescent fingerprint signature was directly observed within the bulk of CQDs/CNC films. Enhanced mechanical stability enables further engineering of these chiral luminescent films *via* chemical and physical patterning technique for fabrication of large area biophotonic materials.



**Scheme 1**. The self-assembly of chiral fluorescent CQDs/CNCs nanostructures.

#### Results and discussion

CNCs are isolated from softwood pulp, and possess needle-like shapes with an average diameter of 4.8±0.6 nm and length of 122±56 nm as measured from AFM height histograms (Figure 1a). 30

CNC aqueous dispersion exhibits long-term stability due to the high surface potential of -51 mV caused by negatively-charged sulfate groups. Two types of CQDs (p-CQDs and o-CQDs) with the size of  $1.5\pm0.5$  nm were synthesized from p- and o-phenylenediamines respectively using a reported solvent-thermal method.<sup>31</sup> These CQDs show blue and yellow fluorescence under 365 nm irradiation, respectively (Figure 1b, Figure S1). As shown in the FTIR spectrum in Figure S2, the as-prepared CQDs contain an abundance of functional groups, including -OH and -NH groups. PEG with a  $M_w$ ~20000 was used to stabilize the CQDs in dispersions.

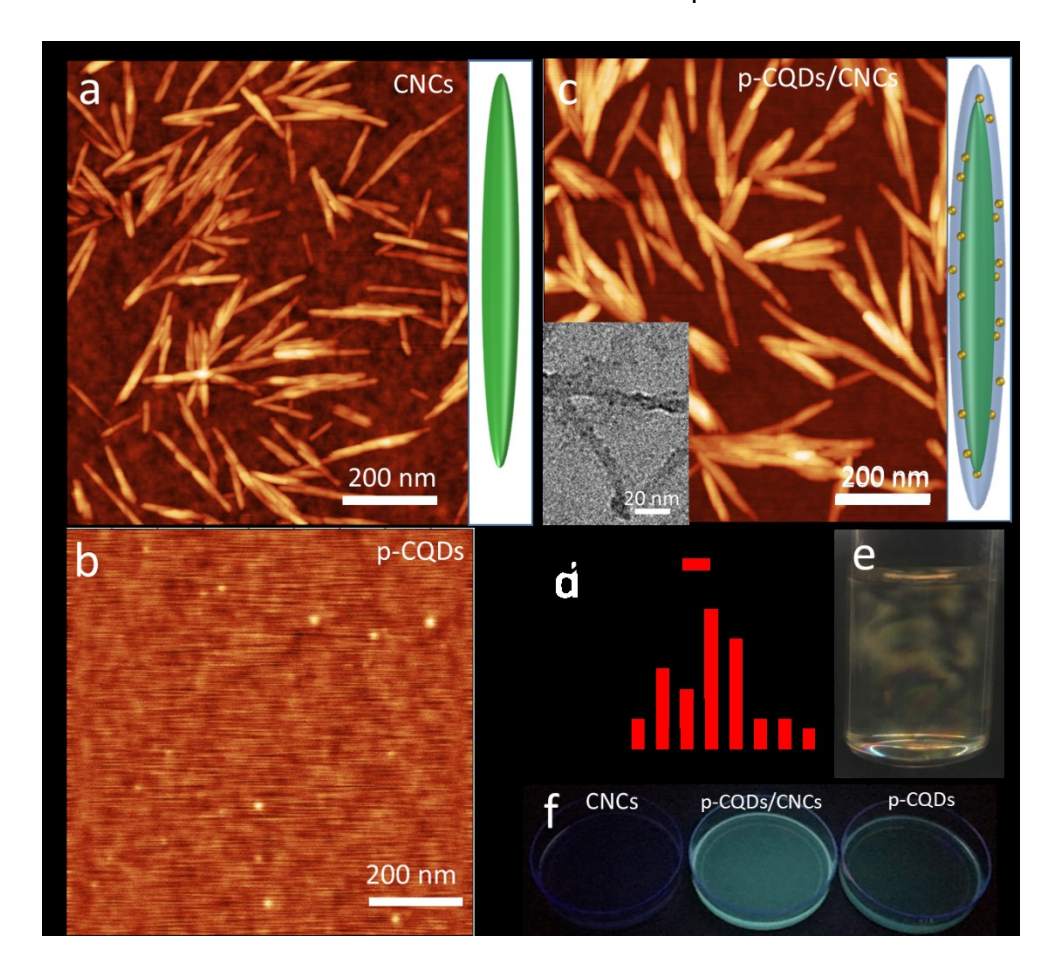


**Figure 1**. Assembly of CQDs/CNCs core/shell nanostructures. AFM images of CNCs (a), p-CQDs (b) and p-CQDs/CNCs containing 50 wt% CQDs (c). Height: 14 nm (a), 3 nm (b) and 16 nm (c). Inset: schemes of CNCs and p-CQDs/CNC core/shell structures; bottom-left inset in c is the high resolution TEM image of p-CQDs/CNC core/shell structures. (d) Diameter distribution of CNCs and p-CQDs/CNCs. (e) Photograph of LC phase of p-CQDs/CNCs dispersions under crossed polarizers. (f) CNCs, p-CQDs and p-CQDs/CNCs dispersions under 365 nm light, where p-CQDs/CNCs dispersion demonstrates enhanced fluorescence.

Combining CQDs with CNCs in an aqueous phase results in a spontaneous formation of uniform core/shell nanostructures (Figure 1c). The high resolution TEM image demonstrates that the

individual CNCs are conformally decorated by CQDs to form core/shell structures (more detail in the SI, Figure S3). However, very small CQD size of 1.5 nm, low electron density contrast, and e-beam damage-prone character compromise spatial resolution and observation of fine details. To further prove this core/shell structure, high resolution AFM characterization was carried out to studied the morphology and size change of CNC after the assembly with CQDs. The resulting effective CQD/CNC diameter increases to 6.1±0.8 nm from the original 4.8±0.6 nm for bare CNCs (Figure 1d, Figure S4), indicating an ultrathin CQD shell with the effective thickness close to CQD diameter around CNCs (see inset in Figure 1c). The formation of core/shell nanostructure was also confirmed by the increase of the effective size from dynamic light scattering (DLS) of CNCs (105 nm) and CQDs/CNCs (170 nm) dispersions that correspond to that expected from about 30% increase in the initial diameter (Figure S5, SI). The decrease of zeta-potential to -40 mV for CQDs/CNCs from -51 mV for bare CNCs further confirms the decoration, as CQDs possess a low zeta-potential of -4.4 mV.

We suggest that this spontaneous assembly is facilitated by complementary heterogeneous amphiphilic interactions between the CNCs and CQDs. As known, CNCs possess an amphiphilic nature because of a combination of hydrophilic (hydroxyl and sulfate groups) and hydrophobic (axial C–H functionalities) facets.<sup>32</sup> The XPS spectra of CQDs indicate the heterogeneous chemistry of CQDs with both hydrophobic C-C/C=C and hydrophilic NH/OH groups presented (Figure S6).<sup>33</sup> Thus, the corresponding amphiphilic character can produce strong hydrophobic-hydrophobic interaction and hydrogen bonding with inherently amphiphilic CNC surface, as demonstrated in the amphiphilic interaction between graphene oxide and CNCs.<sup>7</sup> The presence of the PEG further enhances the interaction between CQDs and CNC acting as a binder due to the strong hydrogen bonding with both CNC and CQD surfaces.<sup>34,35</sup> These amphiphilic interactions resulted in the enhancement of the photoluminescence (PL) of p-CQDs/CNCs dispersion combined with a red-shift in both emission and absorption spectra (Figure 1f, Figures S7 and S8). In addition, two distinct p-CQDs absorption peaks at 237 and 288 nm disappear after adding CNC dispersion due to the band gap shift of p-CQDs (Figure S8), similar with these reported metal ions-CQDs complexes.<sup>36-38</sup>

High negative zeta-potential of CQDs/CNCs facilitates good dispersion stability and stable chiral LC phase in dispersion (Figure 1e), which allow the formation of dried chiral films. The polarized optical microscopy (POM) image of the resulting solid CQDs/CNC film shows characteristic fingerprint-like textures, which is related to the random orientation of the CNC LC tactoids (Figure 2c).<sup>17</sup> The left-handed helicoidal architecture with a pitch distance of around 400 nm can be further

observed by the SEM image of cross-sections of the films (Figure 2f), combined with local highly aligned CQDs/CNCs nanostructures at the film surface (Figure 2e). The chiral morphology gives the p-CQDs/CNCs film a strong CD signal albeit red-shifted to 738 nm when compared to a pure CNC film due to the pitch length increase caused by the presence of the additional PEG/CQD shell (Figure 2g).

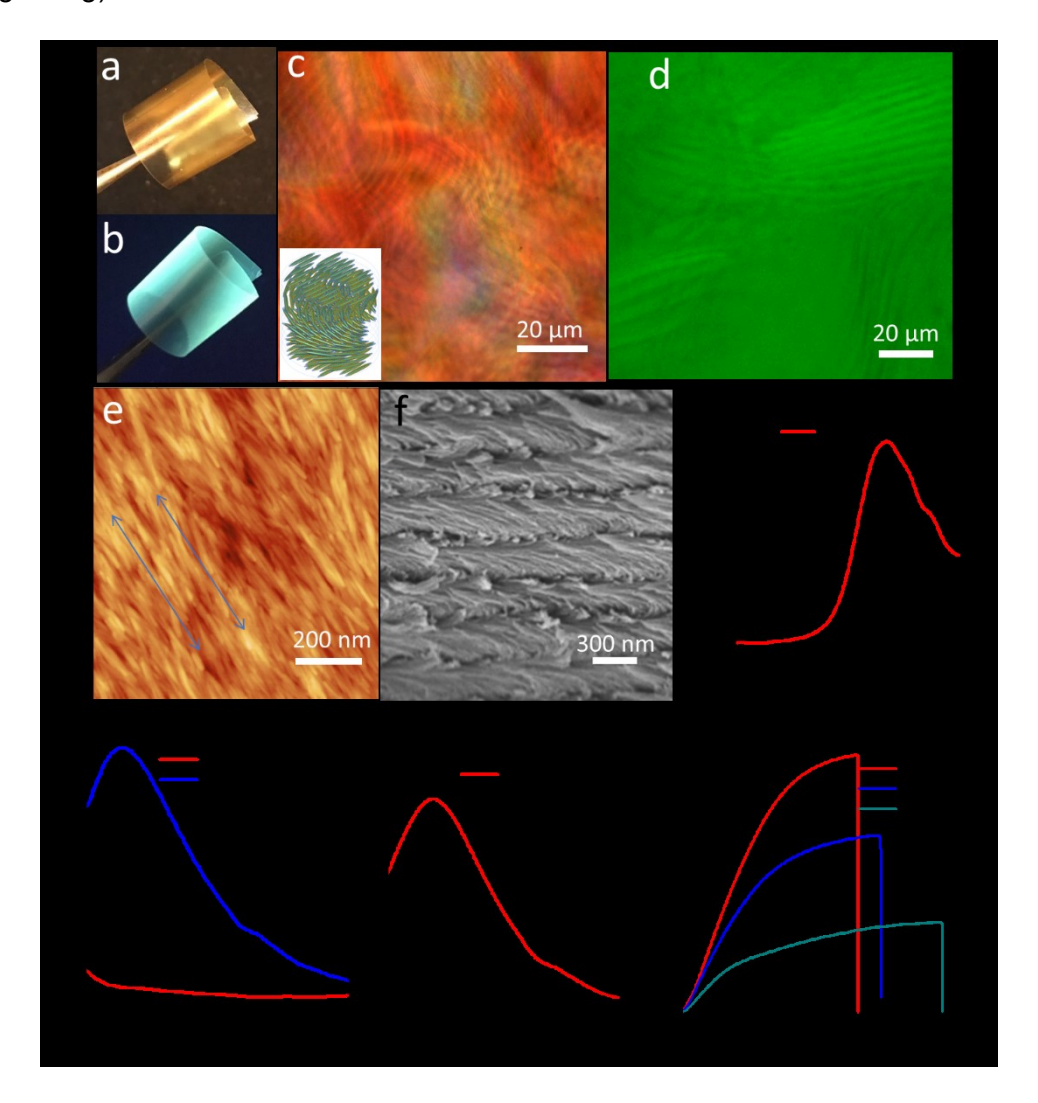


**Figure 2**. Properties of chiral luminescent p-CQDs/CNCs film. Freestanding flexible chiral luminescent p-CQDs/CNCs film containing 50 wt% CQDs under natural light (a) and 365 nm UV light (b). (c) POM image of chiral luminescent p-CQDs/CNCs film, inset: schematic illustration of the helicoidal morphology. (d) Confocal laser scanning luminescence image of p-CQDs/CNCs film, which shows fluorescent fingerprint features originating from self-organized chiral CQDs. (e) AFM image (surface) and (f) SEM image (cross-section) of p-CQDs/CNCs films, arrows indicate the aligning direction of p-CQDs/CNCs (height in AFM image: 35 nm). (g) CD spectra of CNCs film and p-CQDs/CNCs film. (h) PL spectra of p-CQDs, CNC, and p-CQDs/CNCs films. (i)The PL spectra of CQDs/CNC solid films under left- and right-hand (RH and LH) circular polarizers (CP). (j) Representative stress-strain curves of p-CQDs/CNCs films with different CQDs loading.

The broad CD peak indicates the CQDs/CNC film possess chirality at wide range of wavelength. The appearance of a reflection signal with exclusively positive ellipticity confirms the preservation of left-handed chirality after doping with CQDs. 19 The resulting flexible films exhibit brilliant iridescence that originates from the chiral nematic arrangement of CQDs/CNCs superimposed with intense fluorescence (Figure 2a and b). The high fluorescence emission of CQDs/CNC film is due to the fine distribution of CQDs without conventional aggregation (Figures 2h), which can prevent the Förster resonance energy transfer (FRET) based fluorescence quenching. 33 As shown in the control experiment (Figure S9), the CQDs/CNC film without PEG and the CQDs/PEG film without CQDs show negligible fluorescence. Only solid film with co-assembly of these three components (CQDs, CNC and PEG) presents strong fluorescent emission. In this structure, the CNC can act as a template to support CQDs for realizing good distribution, and the presence of PEG can further mediate the CQD interactions for maintaining high fluorescence emission.

As known, high NP loading in CNC films usually results in greatly reduced iridescence and luminescence because of NP aggregation/quenching, distortion of the chiral morphology, and severe phase separation. To determine the effect of CQDs loading on the optical behavior of CNC films, control experiments of CQDs/CNC films with different CQDs loading were carried out. As we observed, in contrast to usual trend, the CQD/CNC films show significant improved iridescence and luminescence even at high CQD loading of 40% (Figure S10, S11). Further increase above 50% of CQDs loading (CQD become a matrix phase) reverse situation and reduce the emission due to the aggregation induced quenching effect. This aggregation effect of the CQDs is confirmed by the emission peak shift from 510 nm to 523 nm when the CQDs loading above 40 wt%.

To prove the chiral fluorescent properties of the CQDs/CNC solid films, we measured the fluorescent spectra of the CQDs/CNC solid films under left- and right-hand circular polarizers. As shown in Figure 2i, the fluorescent intensity of CQDs/CNC solid films in the right-hand (RH) circular polarized channel is significantly higher than the fluorescent intensity in the left-hand (LH) channel. The resulting circular dichroism asymmetric factor of the films, g, is determined to be -0.2, using the eq.  $g = \frac{(I_L - I_R)}{(I_L + I_R)/2}$ , where  $I_L$  and  $I_R$  are the transmitted fluorescence intensity observed in left- or right-hand polarization which is comparable with usual values for other chiral materials.<sup>39</sup> In this evaluation, the negative values indicate RH chiral fluorescence behavior due to the LH chiral organization of the CNC/CQD films.

The confocal fluorescent microscopy was further used to confirm the chiral organization of the CQDs. As known, the chiral nematic CNCs films exhibit characteristic fingerprint patterns in the optical microscopy due to the periodicity in refractive index normal to the axis of the helicoidal arrangement. However, these fingerprint patterns are non-detectable using fluorescent microscopy because of the extremely low fluorescent emission of the pure CNC (Figure S12). In contrast, brilliant fluorescent fingerprint pattern is clearly exhibited in the CQDs/CNC film (Figure 2d), indicating the chiral organization of these materials. Further 3D scanning of the CQDs/CNC film with incremental depth of 50 nm exhibits the continuously spiral structure of individual chiral nematic LC tactoid over tens of micron scale confirming the inclusion of CQDs into integrated chiral organization (see Video S1). This is in contrast to random doping of chiral CNC matrix with fluorescent NPs which usually results in homogenous fluorescence without any fingerprint texture or phase separated of components.<sup>20,25,26</sup>

Additionally, the as-prepared CNC/CQD films demonstrate enhanced mechanical performance because of the plasticizing effect of soft PEG phase.<sup>35</sup> Pure CNC films are brittle and easily cracked under modest bending. After co-assembly with PEG-CQDs components, the resulting CNC films increased the toughness dramatically and became foldable due to both increasing ultimate strength and strain. Significant increase in the ultimate strength [62±5 MPa (CQD/CNC film) vs 40±2 MPa (control CNC film)] and ultimate strain [1.2% (CQD/CNC film) vs 0.6 % (control CNC film)] results in a three-fold higher toughness of ~ 0.50±0.06 MJ/m³ with 10 wt% CQDs loading, combined with the increased elastic modulus of 10±2 GPa (Figure 2j). The fracture morphology of pure CNC and CQDs/CNC films shows significant difference in the reinforcing mechanisms (Figure S13). Smooth fracture surfaces and straight crack growth in pure CNCs films confirms a brittle fracture due to low cohesion of individual CNCs. In contrast, CQD/CNC films show significant plastic deformation and fibril bridge formation supporting the interfacial toughening mechanism via bridge formation. We suggest that CQD-PEG shells around CNCs facilitate strong interfacial binding between neighboring CNCs that allows shearing and reorientation of the helicoidal structures, combined with pulling-out and bridging CNCs bundles. 35,41 This hierarchical deformation can dissipate excessive mechanical energy during ultimate deformation.<sup>25,27</sup>

In comparison with fluorescent CNC materials loaded with semiconducting QDs and organic dyes (Figure S14), 20,25,27,29 our material can realize the chiral organization of CQDs with reduced quenching effect for generating brilliant chiral fluorescence. In the reported fluorescent CNC films, fluorescent components mainly randomly included into the CNC matrix, as proven by the absent

of fluorescent fingerprint patterns (Figure S14f-h). Moreover, the high load of fluorescent components usually causes serious aggregation-induced-fluorescence quenching, resulting in modest fluorescence emission (Figure S14c-g). In contrast, our CQDs/CNC films can significantly minimize the quenching effect because the PEG can stabilize CQDs on the CNC surface to prevent the CQDs aggregation. Additionally, the CQDs/CNC film in this work exhibits superior mechanical integrity and flexibility, which can be repeatable bended and twisted without any cracks because of the plasticizing effect of PEG, in sharp contrast to the extremely brittle behaviors of traditional CNC films (Figure S14b-d).

Finally, we explored high mechanical robustness to fabricate freestanding films with integrated additional optical functionalities *via* soft lithography and chemical printing. As known, patterning of microscopic features into traditional CNC films is challenging and commonly produces catastrophic mechanical failure when lifting CNC films off the templates or using solvents for selective etching and frequently lose chiral organization. In our case, however, directly casting p-CQDs/CNCs LC dispersion on a patterned silicon template can form patterned chiral luminescent films after evaporation-assisted assembly (Figure 3a). The resulting freestanding CQDs/CNC film perfectly replicates the template shape down to sub-micron features and can be lifted without any cracks. The resulting patterns are not only iridescent in natural light, but also are clearly identifiable under UV light because of high local luminescence (Figure 3b and inset in Figure 3e). The silicon templates with a depth of features of 150 nm can be replicated with spatial resolution down to few hundreds of nanometer (Figure 3d and e).

Significantly enhanced vivid structural color with selective reflection can be obtained through constructing large-area diffraction gratings with different periodicities (Figure 3c). These patterned areas exhibit exceptional consistency in optical appearance across the entire area and a combination of light scattering/emission properties from structured surface, helical pitch morphology, and intense photoluminescence which cannot be realized in traditional replicas from optically-neutral synthetic polymers like PDMS. Additionally, construction of grid patterns can generate extensive diffraction patterns with numerous diffraction orders (Figure 3d). Because of the angle-dependent character of diffraction, tuning the view angle of the CNCs film leads to consistent variability of dynamic structural color, which cannot be observed for un-patterned CNC films (see Video S2).

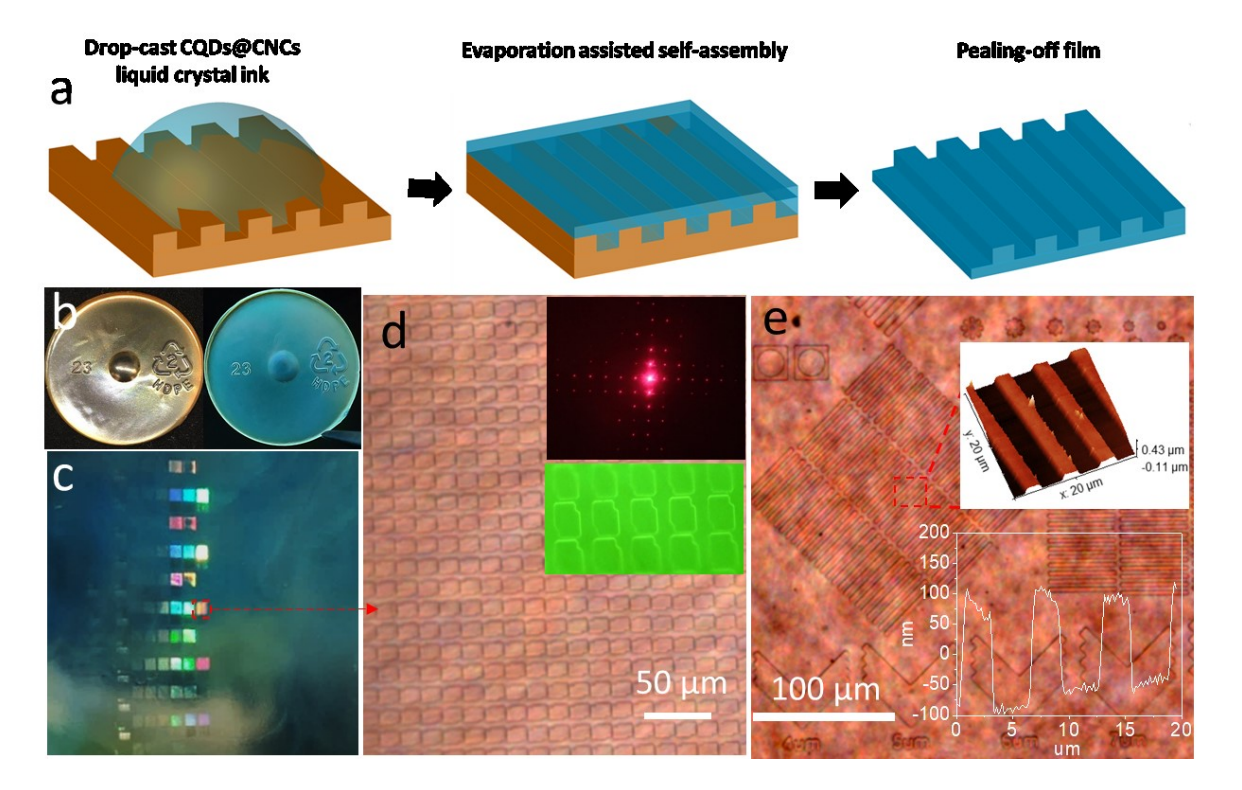


**Figure 3**. Engineering photonic structures on chiral luminescent film. (a) Surface patterning of freestanding chiral luminescent CQD/CNCs films *via* mold casting technique. (b) Macroscopic patterned freestanding CNCs film with 3 cm diameter under natural light (left) and 365 nm UV light (right); (c) Microscopic patterned film with various diffraction gratings. (d) Optical microscopy image of irregular grating, inset: corresponding diffraction pattern and PL image with excitation wavelength of 500 nm. (e) Optical microscopy images of a series of micro-nano patterns with different shapes, inset: 3D AFM image of 5 μm grating and corresponding cross-section profile.

Due to the great potential applications of chiral fluorescent patterns in the sensing and anticounterfeiting, we further developed a chemical 2D printing to generate fluorescent patterns on
freestanding CQD/CNC films (Figure 4a). This approach is facilitated by the peculiar reversible
pH-responsive luminescent behavior of o-CQDs owing to the protonation/deprotonation of the
terminal functional groups (Figure 4b),<sup>33</sup> in contrast to the stable luminescent behavior of p-CQDs
over a wide pH range (Figure S15). As a result, the iridescent films assembled from oCQDs/CNCs dispersions show no luminescence because of the acidic condition at pH of 3.3.
However, it can be immediately recovered by localized alkali treatment of the CQD/CNC films
(Figure S16). Inkjet printing can be utilized to deliver droplets to initiate such a localized change
from acidic to alkali state to restore local luminescence and, thus, to generate printed emissive
patterns (Figure 4a). The resulting untreated areas remain iridescent and non-emissive while the
highly luminescent and scattered printed-in local patterned areas can be clearly observed (Figure

4c). The scattering contrast might be caused by the refractive index contrast due to the presence of residual salt in the patterned area. Under UV light excitation, well-defined luminescent patterns are presented with high fluorescent emission (Figure 4d). These chiral fluorescent patterns are unprocurable using direct inkjet printing CQDs/CNC ink because a high shearing force of printing would generally destroy the chiral structure. Compared with other conventional patterning techniques, this technique shows advantages in low-cost, large-scale fabrication, and high efficiency.

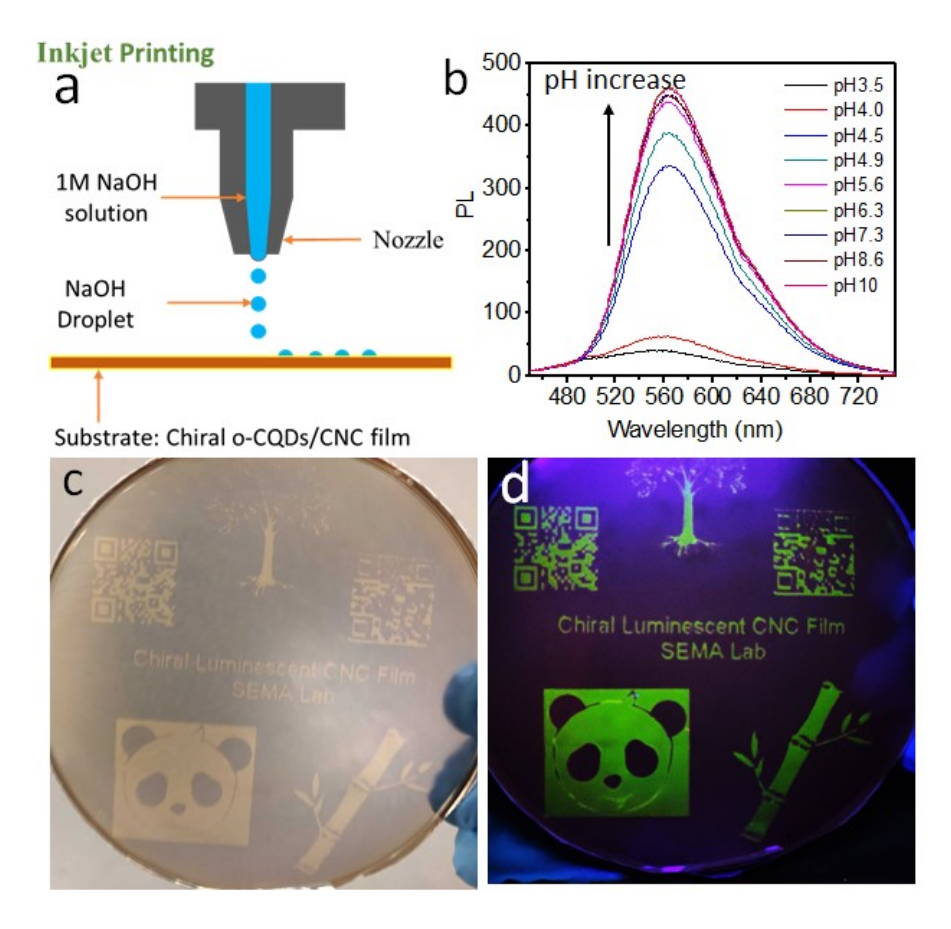


**Figure 4**. (a) Inkjet printing of chemically patterned chiral luminescent CNCs films. (b) PL spectra of o-CQDs dispersion in different pH environment. Patterned chiral luminescent CNCs films with diameter of 10 cm under natural light (c) and at 365 nm UV light (d) (Patterns are designed by the authors).

#### **Conclusions**

In conclusion, we reported a self-assembled emissive CQD-decorated CNC nanostructure for constructing flexible robust chiral fluorescent materials. Heterogeneous amphiphilic interactions allow spontaneous decoration of polymer-stabilized CQDs around the CNC 1D nanostructures.

This hybrid nanostructure can self-organize into fluorescent chiral LC phase and subsequent preservation of this chiral morphology in flexible solid CNC films. The resulting film demonstrates a characteristic fluorescent fingerprint signature that has never been observed for claimed chiral films. This feature proves that the core/shell nanostructures assembled in this work allow CQD/CNCs to form chiral morphologies, rather than randomly distributing in the CNC matrix. As a result, the solid chiral CQDs/CNC film demonstrate right-hand chiral fluorescence with an asymmetric factor of -0.2. Additionally, the robust freestanding CQDs/CNC films show dramatically enhanced fluorescence that are significantly higher than that for pure CQD films and reported CQDs/CNC films. Enhanced structural colors with selective light reflection and emissive fluorescent patterns can be further realized *via* soft lithography and 2D chemical printing. The combination of chiral fluorescence with photonic behavior is promising for biophotonic applications, such as anti-counterfeiting, waveguiding, lasing, and optical vortex control.

#### **Materials and Methods**

# **Preparation of CNCs dispersion**

The synthesis of CNCs were carried out using well-established sulfuric acid methods.<sup>30</sup> Briefly, dried soft wood pulp (17 g) was slowly added in 420 g sulfuric acid (64 wt%) for hydrolyzing 90 min under vigorous stirring. The reaction temperature is 45°C. The above yellow mixture was added into 1500 mL cold DI water to stop the hydrolysis, and purified by centrifuging at 6000 rpm for 10 min. The resulting CNCs dispersion were placed into dialysis tube against DI water for further removal of CNCs. After dialysis of a week, the CNCs were centrifuged at 10000 rpm for 20 min to remove aggregation and thick wood fibers. The resulting well-dispersed CNCs supernatant (0.4 wt%) was sonicated for 3 min using (Qsonica Q125, 125 W) at 50% amplitude for further characterization and self-assembly.

# **Preparation of CQDs dispersion**

CQDs were synthesized according to a previous study.<sup>31</sup> o- and p-phenylenediamines (0.90 g) was firstly dissolved in 90 mL ethanol respectively, and then the solutions was transferred into poly(tetrafluoroethylene)-lined autoclaves. After heating at 180 °C in oven for 12 h and cooling down to room temperature naturally, yellow and blue CQDs suspensions were obtained from o- and p-phenylenediamines, respectively. The as-prepared p-CQDs are basically amorphous as demonstrated in the XRD spectra (Figure S17). The fluorescence quantum yield of p-CQDs in the

dispersion to be around 1% using the quinine sulfate (quantum yield = 54%) were chosen as standard reference.<sup>44</sup> To stabilize CQDs, the above CQDs dispersions (1mL, 1 wt%) were added into 20 mL PEG aqueous solution (Mw~ 20000, 5 wt%), and dried in oven at 80 °C overnight before redissolved in 20 ml nanopure water. The resulting PEG stabilized CQDs will be used for the preparation of chiral luminescent films.

# **Construction of chiral luminescent CNCs films**

Typically, 0.8 mL PEG stabilized p-CQDs (5 wt%) was added into 20 mL CNCs (0.4 wt%) for forming the core/shell structure. Then, the mixture was added into plastic petri dish (60 x 15 mm) to allow the solvent evaporation induced self-assembly in ambient environment. The mixture will self-assemble into iridescent and luminescent solid film after two days. The resulting solid films contain about 0.08 g CNC, 0.04g PEG and 0.004g CQDs. To surface engineer the chiral luminescent film, p-CQDs/CNC liquid crystal ink (around 3 wt%) with 30 wt% CQDs loading is dropped cast on hydrophobic silicon wafer that was patterned by photolithography. After drying, this patterned chiral luminescent film can be peeled off to obtain free-standing film. To chemical pattern the chiral luminescent film, we use an inkjet printer (JetLabII Ink-jet Printer) filled with 1M NaOH to pattern the free-standing o-CQDs/CNC film.

#### Characterization

Atomic force microscopy (AFM) images with resolution of 512 x 512 pixels were captured by AFM (ICON, Bruker) with soft tapping mode at 0.7 Hz in usual manner.<sup>45</sup> To character the size of CQDs/CNCs, CQDs/CNCs dispersion was spun cast on piranha solution treated silicon wafer at speed of 3000 rpm. The average length and diameter distribution of CQDs/CNCs was determined from the AFM images using Gwyddion software. Scanning electron microscope (SEM) was performed on Hitachi SU-8230, using 5 kV accelerating voltage. TEM imaging was conducted on a Hitachi HT7700 by dropcast the sample onto a carbon-Formvar TEM grid (TED PELLA, INC). To minimize radiation damage and use the smallest objective aperture for enhancing contrast, measurements were operated at 120 kV acceleration voltage. Universal tensile tester (Shimadzu EZ-SX 500 N) was used to measure the tensile stress-strain curves of CQDs/CNCs films with speed of 0.1 mm/min. Surface potentials (zeta ( $\zeta$ ) – potential) and hydrodynamic sizes were obtained with a Malvern Zetasizer Nano ZS for dynamic light scattering (DLS) and electrophoretic light scattering (ELS) with 173° scattering angle. Polarized optical microscopy (POM) images were obtained with an Olympus BX51 microscope in the reflection mode with crossed polarizers. CD spectrum was collected using Applied Photophysics Chirascan plus. Optical properties were analyzed using UV-vis (Shimadzu 3600plus) and home-made micro reflection detector that is

capable of measuring localized reflection of CNC films with resolution of 10 um. Fluorescence of CQDs/CNCs films were characterized using Shimadzu UV 2450. Confocal images and video were obtained with a LSM 510 Vis confocal microscope equipped with a 63 ×1.4 oil immersion objective lens (Zeiss) and scan depth of 50 nm for each layer. XRD data were collected with XPert Pro Alpha-1 diffractometer. XPS spectra were obtained with a Thermal Scientific K-alpha XPS instrument.

# **Supporting Information**

The Supporting Information is available free of charge on the ACS Publications website at DOI:......

Figures S1–S17: AFM, PL spectra, FTIR, XPS and XRD of CQDs; TEM and AFM images of CQDs/CNC; DLS size distribution, PL and UV-vis spectra of CQDs/CNC; photos of CQDs/CNC films different CQDs loading under natural light and UV light; PL spectra and PL intensity of CQDs/CNC films with different CQDs loading; fluorescent microscopy image of CNC and CQDs/CNCs films; SEM fracture images of CNCs film and CQDs/CNCs film; Comparison of the fluorescent images of CQDs/CNC film with reported chiral fluorescent CNC films; The pH-stable behavior of p-CQDs/CNC dispersion; photos of iridescent o-CQDs/CNCs film after 1M NaOH treatment under natural light and 365 UV light.

Supplemental Video S1: Confocal laser scanning microscopy images of fluorescent fingerprint signature that is derived from the chiral organization of CQDs.

Supplemental Video S2: Dynamic structural color of the pattered flexible chiral fluorescent film.

# **Acknowledgments**

This work was supported by Air Force Research Lab FA8650-D-16-5404, Air Force Office for Scientific Research FA9550-17-1-0297, and NSF CBET-1803495 Awards.

#### References

1 Ma, W.; Xu, L.; de Moura, A. F.; Wu, X.; Kuang, H.; Xu, C.; Kotov, N. A. Chiral Inorganic Nanostructures. *Chem. Rev.* **2017**, *117*, 8041–8093.

- 2 Wu, X.; Hao, C.; Kumar, J.; Kuang, H.; A. Kotov, N.; M. Liz-Marzán, L.; Xu, C. Environmentally Responsive Plasmonic Nanoassemblies for Biosensing. *Chem. Soc. Rev.* **2018**, *47*, 4677–4696.
- 3 Kuzyk, A.; Schreiber, R.; Fan, Z.; Pardatscher, G.; Roller, E.-M.; Högele, A.; Simmel, F. C.; Govorov, A. O.; Liedl, T. DNA-Based Self-Assembly of Chiral Plasmonic Nanostructures with Tailored Optical Response. *Nature* **2012**, *483*, 311–314.
- 4 Wu, X.; Xu, L.; Liu, L.; Ma, W.; Yin, H.; Kuang, H.; Wang, L.; Xu, C.; Kotov, N. A. Unexpected Chirality of Nanoparticle Dimers and Ultrasensitive Chiroplasmonic Bioanalysis. *J. Am. Chem. Soc.* **2013**, *135*, 18629–18636.
- 5 Yan, W.; Xu, L.; Xu, C.; Ma, W.; Kuang, H.; Wang, L.; Kotov, N. A. Self-Assembly of Chiral Nanoparticle Pyramids with Strong R/S Optical Activity. *J. Am. Chem. Soc.* **2012**, *134*, 15114–15121.
- 6 Suzuki, N.; Wang, Y.; Elvati, P.; Qu, Z.-B.; Kim, K.; Jiang, S.; Baumeister, E.; Lee, J.; Yeom, B.; Bahng, J. H.; Lee, J.; Violi, A.; Kotov, N. A.; Chiral Graphene Quantum Dots. *ACS Nano* **2016**, *10*, 1744–1755.
- 7 Xiong, R.; Kim, H. S.; Zhang, L.; Korolovych, V. F.; Zhang, S.; Yingling, Y. G.; Tsukruk, V. V. Wrapping Nanocellulose Nets around Graphene Oxide Sheets. *Angew. Chem.* **2018**, *130*, 8644–8649.
- 8 Xiong, R.; Kim, H. S.; Zhang, S.; Kim, S.; Korolovych, V. F.; Ma, R.; Yingling, Y. G.; Lu, C.; Tsukruk, V. V. Template-Guided Assembly of Silk Fibroin on Cellulose Nanofibers for Robust Nanostructures with Ultrafast Water Transport. *ACS Nano* **2017**, *11*, 12008-12019.
- 9 Golmohammadi, H.; Morales-Narváez, E.; Naghdi, T.; Merkoçi, A. Nanocellulose in Sensing and Biosensing. *Chem. Mater.* **2017**, 29, 5426–5446.
- 10 Thomas, B.; Raj, M. C.; Athira, K. B; Rubiyah, M. H; Joy, J.; Moores, A.; Drisko, G. L.; Sanchez, C. Nanocellulose, a Versatile Green Platform: From Biosources to Materials and Their Applications. *Chem. Rev.* **2018**, 118, 11575-11625.
- 11 Xiong, R.; Grant, A. M.; Ma, R.; Zhang, S.; Tsukruk, V. V. Naturally-Derived Biopolymer Nanocomposites: Interfacial Design, Properties and Emerging Applications. *Mater. Sci. Eng. R Rep.* **2018**, *125*, 1–41.
- 12 Klemm, D.; Kramer, F.; Moritz, S.; Lindström, T.; Ankerfors, M.; Gray, D.; Dorris, A. Nanocelluloses: A New Family of Nature-Based Materials. *Angew. Chem. Int. Ed.* **2011**, *50*, 5438–5466.
- 13 Moon, R. J.; Martini, A.; Nairn, J.; Simonsen, J.; Youngblood, J. Cellulose Nanomaterials Review: Structure, Properties and Nanocomposites. *Chem. Soc. Rev.* **2011**, *40*, 3941–3994.
- 14 Kontturi, E.; Laaksonen, P.; Linder, M. B.; Nonappa; Gröschel, A. H.; Rojas, O. J.; Ikkala, O. Advanced Materials through Assembly of Nanocelluloses. *Adv. Mater.* **2018**, *30*, 1703779.
- 15 Lagerwall, J. P.; Schütz, C.; Salajkova, M.; Noh, J.; Park, J. H.; Scalia, G.; Bergström, L. Cellulose Nanocrystal-Based Materials: From Liquid Crystal Self-Assembly and Glass Formation to Multifunctional Thin Films. *NPG Asia Mater.* **2014**, *6*, e80.
- 16 Habibi, Y.; Lucia, L. A.; Rojas, O. J. Cellulose Nanocrystals: Chemistry, Self-Assembly, and Applications. *Chem. Rev.* **2010**, *110*, 3479–3500.
- 17 Parker, R. M.; Guidetti, G.; Williams, C. A.; Zhao, T.; Narkevicius, A.; Vignolini, S.; Frka-Petesic, B. The Self-Assembly of Cellulose Nanocrystals: Hierarchical Design of Visual Appearance. *Adv. Mater.* **2018**, *30*, 1704477.
- 18 Cherpak, V.; Korolovych, V. F.; Geryak, R.; Turiv, T.; Nepal, D.; Kelly, J.; Bunning, T. J.; Lavrentovich, O. D.; Heller, W. T.; Tsukruk, V. V. Robust Chiral Organization of Cellulose Nanocrystals in Capillary Confinement. *Nano Lett.* **2018**, *18*, 6770–6777.
- 19 Giese, M.; Blusch, L. K.; Khan, M. K.; MacLachlan, M. J. Functional Materials from Cellulose-Derived Liquid-Crystal Templates. *Angew. Chem. Int. Ed.* **2015**, *54*, 2888–2910.

- 20 Thérien-Aubin, H.; Lukach, A.; Pitch, N.; Kumacheva, E. Coassembly of Nanorods and Nanospheres in Suspensions and in Stratified Films. *Angew. Chem. Int. Ed.* **2015**, *54*, 5618–5622.
- 21 Li, Y.; Prince, E.; Cho, S.; Salari, A.; Golestani, Y. M.; Lavrentovich, O. D.; Kumacheva, E. Periodic Assembly of Nanoparticle Arrays in Disclinations of Cholesteric Liquid Crystals. *Proc. Natl. Acad. Sci.* **2017**, *114*, 2137–2142.
- 22 Querejeta-Fernández, A.; Chauve, G.; Methot, M.; Bouchard, J.; Kumacheva, E. Chiral Plasmonic Films Formed by Gold Nanorods and Cellulose Nanocrystals. *J. Am. Chem. Soc.* **2014**, *136*, 4788–4793.
- 23 Querejeta-Fernández, A.; Kopera, B.; Prado, K. S.; Klinkova, A.; Methot, M.; Chauve, G.; Bouchard, J.; Helmy, A. S.; Kumacheva, E. Circular Dichroism of Chiral Nematic Films of Cellulose Nanocrystals Loaded with Plasmonic Nanoparticles. *ACS Nano* **2015**, 9, 10377–10385.
- 24 Rofouie, P.; Alizadehgiashi, M.; Mundoor, H.; Smalyukh, I. I.; Kumacheva, E. Self-Assembly of Cellulose Nanocrystals into Semi-Spherical Photonic Cholesteric Films. *Adv. Funct. Mater.* **2018**, *28*, 1803852.
- 25 Nguyen, T.-D.; Hamad, W. Y.; MacLachlan, M. J. CdS Quantum Dots Encapsulated in Chiral Nematic Mesoporous Silica: New Iridescent and Luminescent Materials. *Adv. Funct. Mater.* **2014**, *24*, 777–783.
- 26 Chu, G.; Wang, X.; Chen, T.; Xu, W.; Wang, Y.; Song, H.; Xu, Y. Chiral Electronic Transitions of YVO 4:Eu 3+ Nanoparticles in Cellulose Based Photonic Materials with Circularly Polarized Excitation. *J. Mater. Chem. C* **2015**, *3*, 3384–3390.
- 27 Lizundia, E.; Nguyen, T.-D.; Vilas, J. L.; Hamad, W. Y.; MacLachlan, M. J. Chiroptical Luminescent Nanostructured Cellulose Films. *Mater. Chem. Front.* **2017**, *1*, 979–987.
- 28 Guidetti, G.; Atifi, S.; Vignolini, S.; Hamad, W. Y. Flexible Photonic Cellulose Nanocrystal Films. *Adv. Mater.* 28, 10042–10047.
- 29 Zheng, H.; Ju, B.; Wang, X.; Wang, W.; Li, M.; Tang, Z.; Zhang, S.; Xu, Y. Circularly Polarized Luminescent Carbon Dot Nanomaterials of Helical Superstructures for Circularly Polarized Light Detection. *Adv. Optical Mater.* **2018**, *6*, 1801246.
- 30 Beck-Candanedo, S.; Roman, M.; Gray, D. G. Effect of Reaction Conditions on the Properties and Behavior of Wood Cellulose Nanocrystal Suspensions. *Biomacromolecules* **2005**, *6*, 1048–1054.
- 31 Jiang, K.; Sun, S.; Zhang, L.; Lu, Y.; Wu, A.; Cai, C.; Lin, H. Red, Green, and Blue Luminescence by Carbon Dots: Full-Color Emission Tuning and Multicolor Cellular Imaging. *Angew. Chem. Int. Ed.* **2015**, *54*, 5360–5363.
- 32 Fernandes, A. N.; Thomas, L. H.; Altaner, C. M.; Callow, P.; Forsyth, V. T.; Apperley, D. C.; Kennedy, C. J.; Jarvis, M. C. Nanostructure of Cellulose Microfibrils in Spruce Wood. *Proc. Natl. Acad. Sci.* **2011**, *108*, E1195–E1203.
- 33 Sinko, R.; Qin, X.; Keten, S. Interfacial Mechanics of Cellulose Nanocrystals. *MRS Bull.* **2015**, 40, 340–348.
- 34 Sun, Y.-P.; Zhou, B.; Lin, Y.; Wang, W.; Fernando, K. A. S.; Pathak, P.; Meziani, M. J.; Harruff, B. A.; Wang, X.; Wang, H.; Luo, P.G.; Yang, H.; Kose, M. E.; Chen, B.; Veca, L. M.; Xie, S.-Y. Quantum-Sized Carbon Dots for Bright and Colorful Photoluminescence. *J. Am. Chem. Soc.* **2006**, *128*, 7756–7757.
- 35Yao, K.; Meng, Q.; Bulone, V.; Zhou, Q. Flexible and Responsive Chiral Nematic Cellulose Nanocrystal/Poly(Ethylene Glycol) Composite Films with Uniform and Tunable Structural Color. *Adv. Mater.* **2017**, *29*, 1701323.
- 36 Zhu, S.; Song, Y.; Zhao, X.; Shao, J.; Zhang, J.; Yang, B. The Photoluminescence Mechanism in Carbon Dots (Graphene Quantum Dots, Carbon Nanodots, and Polymer Dots): Current State and Future Perspective. *Nano Res.* **2015**, *8*, 355–381.

- 37 Zhang, R.; Chen, W. Nitrogen-Doped Carbon Quantum Dots: Facile Synthesis and Application as a "Turn-off" Fluorescent Probe for Detection of Hg<sup>2+</sup> Ions. *Biosens. Bioelectron.* **2014**, *55*, 83–90.
- 38 Dong, Y.; Wang, R.; Li, G.; Chen, C.; Chi, Y.; Chen, G. Polyamine-Functionalized Carbon Quantum Dots as Fluorescent Probes for Selective and Sensitive Detection of Copper Ions. *Anal. Chem.* **2012**, *84*, 6220–6224.
- 39 Tang, Y.; Cohen, A. E. Enhanced Enantioselectivity in Excitation of Chiral Molecules by Superchiral Light. *Science* **2011**, *332* (6027), 333–336.
- 40 Habibi, Y.; Lucia, L. A.; Rojas, O. J. Cellulose Nanocrystals: Chemistry, Self-Assembly, and Applications. *Chem. Rev.* **2010**, *110* (6), 3479–3500.
- 41 Xiong, R.; Hu, K.; Grant, A. M.; Ma, R.; Xu, W.; Lu, C.; Zhang, X.; Tsukruk, V. V. Ultrarobust Transparent Cellulose Nanocrystal-Graphene Membranes with High Electrical Conductivity. *Adv. Mater.* **2016**, *28*, 1501–1509.
- 42 Espinha, A.; Dore, C.; Matricardi, C.; Alonso, M. I.; Goñi, A. R.; Mihi, A. Hydroxypropyl Cellulose Photonic Architectures by Soft Nanoimprinting Lithography. *Nat. Photonics* **2018**, *12*, 343-384.
- 43 Zhou, Y.; Li, Y.; Dundar, F.; Carter, K. R.; Watkins, J. J. Fabrication of Patterned Cellulose Film *via* Solvent-Assisted Soft Nanoimprint Lithography at a Submicron Scale. *Cellulose* **2018**, 25. 5185-5194.
- 44 Zhu, S.; Meng, Q.; Wang, L.; Zhang, J.; Song, Y.; Jin, H.; Zhang, K.; Sun, H.; Wang, H.; Yang, B. Highly Photoluminescent Carbon Dots for Multicolor Patterning, Sensors, and Bioimaging. *Angew. Chem. Int. Ed.* **2013**, *52*, 3953–3957.
- 45 McConney, M. E.; Singamaneni, S.; Tsukruk, V. V. Probing Soft Matter with the Atomic Force Microscopies: Imaging and Force Spectroscopy. *Polym. Rev.* **2010**, 50, 235–286.

# тос

